Journal of Materials Chemistry A

ROYAL SOCIETY OF CHEMISTRY

PAPER

View Article Online
View Journal | View Issue

Cite this: J. Mater. Chem. A, 2023, 11, 25386

Cu-ATC *vs.* Cu-BTC: comparing the H_2 adsorption mechanism through experiment, molecular simulation, and inelastic neutron scattering studies†

Tony Pham, ‡*[a] Katherine A. Forrest,‡[a] Zheng Niu,[b] Brant Tudor,[a] Chloe B. Starkey,[a] Yue Wang,[b] Mohamed Eddaoudi,[c] Nathaniel Rosi,[d] Gisela Orcajo,[e] Juergen Eckert, *[af] Shengqian Ma[g] and Brian Space *[ah]

A combined experimental, inelastic neutron scattering (INS), and theoretical study of H_2 adsorption was carried out in Cu-ATC and Cu-BTC, two metal–organic frameworks (MOFs) that consist of Cu^{2+} ions coordinated to 1,3,5,7-adamantanetetracarboxylate (ATC) and 1,3,5-benzenetricarboxylate (BTC) linkers, respectively. Experimental measurements revealed that Cu-ATC exhibits higher H_2 uptake at low pressures than Cu-BTC, but saturates more quickly on account of its lower surface area. This results in a higher isosteric heat of adsorption (Q_{st}) value at zero-coverage for Cu-ATC (12.63 kJ mol^{-1}). Grand canonical Monte Carlo (GCMC) simulations of H_2 adsorption in both MOFs produced isotherms that are in outstanding agreement with the corresponding experimental measurements at 77 and 87 K and pressures up to 1 atm. The simulations revealed that the H_2 molecules initially bind onto the Cu^{2+} ions of the copper paddlewheel ($[Cu_2(O_2CR)_4]$) units in both MOFs. In Cu-ATC, however, a H_2 molecule can interact with two Cu^{2+} ions of adjacent paddlewheels simultaneously, which provides for a favorable, synergistic interactions. The INS spectra of H_2 adsorbed in Cu-ATC and Cu-BTC showed neutron energy transfer peaks occurring at approximately 7.5 and 8.9 meV, respectively; these peaks correspond to the binding of H_2 onto the open-metal sites in both MOFs. The lower energy peak for Cu-ATC indicates that the adsorbed H_2 molecules experience a higher barrier to rotation and a stronger interaction with the host relative to Cu-BTC. These results were supported by two-dimensional quantum rotation calculations. This study demonstrates how differences in the H_2 adsorption mechanism between two prototypal MOFs with copper paddlewheel units can be discerned through a combination of experimental measurements and theoretical calculations.

Received 9th August 2023
Accepted 11th October 2023

DOI: 10.1039/d3ta04748b

rsc.li/materials-a

1. Introduction

Metal–organic frameworks (MOFs) are three-dimensional structures that are synthesized by combining metal ions with organic ligands. Their often porous nature gives them the ability to adsorb a variety of guest molecules, and thus, allowing them to become suitable materials for applications in gas adsorption and separation. For instance, MOFs have been considered to be promising candidates to approach the U.S. Department of Energy (DOE) targets for H_2 storage.[1,2] Hydrogen

[a]Department of Chemistry, University of South Florida, 4202 East Fowler Avenue, CHE205, Tampa, Florida 33620-5250, USA. E-mail: tpham4@mail.usf.edu; juergen@usf.edu; bspace@ncsu.edu

[b]College of Chemistry, Chemical Engineering and Materials Science, Soochow University, Suzhou, Jiangsu 215123, People's Republic of China

[c]Advanced Membranes and Porous Materials Center, Division of Physical Sciences and Engineering, 4700 King Abdullah University of Science and Technology, Thuwal 23955-6900, Kingdom of Saudi Arabia

[d]Department of Chemistry, University of Pittsburgh, Chevron Science Center, 219 Parkman Avenue, Pittsburgh, Pennsylvania 15260, USA

[e]Department of Chemical and Energy Technology, ESCET, Rey Juan Carlos University, C/Tulipán s/n, 28933 Móstoles, Madrid, Spain

[f]Department of Chemistry and Biochemistry, Texas Tech University, 2500 Broadway, Box 41061, Lubbock, Texas 79409-1061, USA

[g]Department of Chemistry, University of North Texas, 1508 West Mulberry Street, Denton, Texas 76201, USA

[h]Department of Chemistry, North Carolina State University, 2700 Stinson Drive, Cox Hall 506, Raleigh, North Carolina 27607, USA

† Electronic supplementary information (ESI) available: Tables containing partial charges, pictures of MOF fragments, details of synthesis and characterization, details of isosteric heat of adsorption, periodic density functional theory, and quantum rotation calculations, details of cycling performance experiments, and additional experimental and simulated results. See DOI: https://doi.org/10.1039/d3ta04748b

‡ Authors contributed equally.

storage in MOFs is based on physisorption, where the interaction energy between the H_2 molecule and the framework is rather weak (*ca.* 5.0 to 50.0 kJ mol^{-1}). MOFs can adsorb a substantial amount of H_2 within the pores and have the ability to release the molecules facilely through changes in thermodynamic conditions.

Although a major goal in this hydrogen economy is to find a material that can store a considerable amount of H_2 at room temperature and high pressures, evaluating H_2 adsorption in MOFs at low pressures (<0.01 atm) is typically important to assess the interaction strength between the H_2 molecules and the framework when the adsorbates first enter the material. Thus, even though low-pressure H_2 storage does not provide a quantitative measure of the H_2 uptake capacity in a MOF under practical conditions, studying this region can still yield insights into the energetics of the H_2 binding sites in the material. This is especially since a more accurate determination of the initial isosteric heat of adsorption (Q_{st}) for H_2 can be made when investigating H_2 adsorption under these conditions as such values at zero-coverage depend on the H_2 uptake at low pressures. It is expected that any material that can meet the U.S. DOE targets for onboard H_2 storage would exhibit a H_2 Q_{st} within the range of 15–30 kJ mol^{-1}.[3,4]

A large number of MOFs have been synthesized over the past two decades and were studied for their hydrogen adsorption properties. Cu-BTC (also known as HKUST-1) is a prototypal MOF that has been extensively studied for H_2 adsorption.[5–10] This MOF is synthesized by combining Cu^{2+} ions with the relatively simple 1,3,5-benzenetricarboxylate (BTC) ligand (Fig. 1(b) and (d)).[11] In the structure of this MOF, the Cu^{2+} ions coordinate to the oxygen atoms of the ligand to form the copper paddlewheel, $[Cu_2(O_2CR)_4]$, clusters. The as-synthesized version of the MOF contains a solvent molecule that is coordinated to the axial position of each Cu^{2+} ion. The solvent molecules can be removed through various activation processes to leave exposed Cu^{2+} ions on the paddlewheels. These Cu^{2+} ions serve as an open-metal site, which is an energetically favorable site for the H_2 molecules. Various hydrogen adsorption measurements on Cu-BTC revealed that the initial Q_{st} value for H_2 in this MOF ranges from 6.0 to 7.0 kJ mol^{-1}, which is associated with adsorption directly onto the open-metal sites.[5–10]

Information on the energetics about each H_2 binding site in a MOF can be obtained by performing inelastic neutron scattering (INS) studies for H_2 in the material.[12–17] The resulting INS spectra contains a number of distinct peaks, with most peaks corresponding to a particular H_2 adsorption site in the MOF. The presence of these peaks in the spectra is mainly due to the rotational excitations of the H_2 molecules as they are adsorbed about a specific site in the MOF. In vacuum, a H_2 molecule rotates freely with energy levels that are representative of a rigid rotor; the lowest transition occurs at 14.7 meV, which is the transition between ortho- and para-H_2. In the presence of an external field, such as a MOF adsorption site, a barrier to rotation is imparted on the H_2 molecule as the $(2j + 1)$ degeneracy is lifted, thus causing the energies of each j level to split.

Earlier INS studies of H_2 adsorbed in Cu-BTC by Brown *et al.*[18] revealed a peak that occurs at about 9.0 meV for different loadings of H_2; this is the lowest energy transfer peak for H_2 in the MOF. Peaks that appear at lower energies in the INS spectra correspond to higher rotational barriers and hence, stronger interactions at a particular binding site within the host material. As explained in ref. 18, this 9.0 meV peak observed in the INS spectra for Cu-BTC corresponds to the adsorption of H_2 onto the open-metal Cu^{2+} ions. This was verified through calculating the rotational energy levels for a H_2 molecule adsorbed about the copper paddlewheels through generalized gradient approximation (GGA) calculations.[19]

A number of different MOFs containing copper paddlewheel clusters have been synthesized by combining Cu^{2+} ions with a certain carboxylate-based ligand.[20] Cu-BTC remains the most

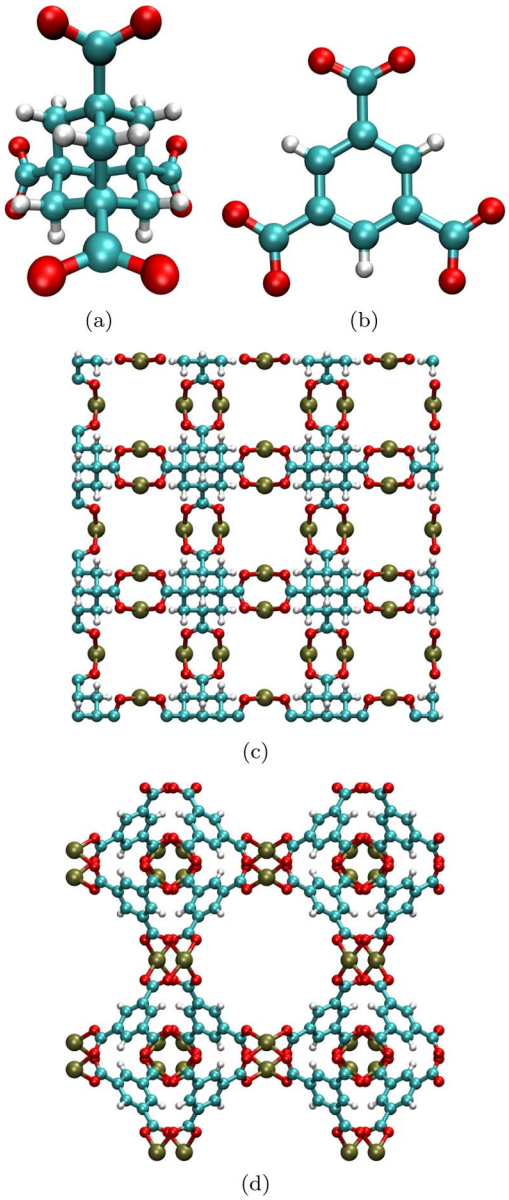

Fig. 1 (a) 1,3,5,7-Adamantanetetracarboxylate (ATC) and (b) 1,3,5-benzenetricarboxylate (BTC) ligand used to synthesize (c) Cu-ATC (orthographic *c*-axis view of 3 × 3 × 2 supercell) and (d) Cu-BTC (orthographic *c*-axis view of a single unit cell), respectively.

well-known and simplest MOF that contain such copper paddlewheel units as it is synthesized using an elementary ligand that is commercially available. A ligand that represents a higher dimensional version of BTC is 1,3,5,7-adamantanetetracarboxylate (ATC) (Fig. 1(a)).[21] The ATC ligand exhibits a diamond-like structure, where the adamantane unit can be viewed as a tetrahedral building block. Compared to other tetracarboxylate ligands,[22–25] ATC is the smallest ligand containing four carboxylate groups (and representing a tetrahedral node) that can be used to synthesize a MOF containing copper paddlewheels. Indeed, the combination of Cu^{2+} ions with ATC yields the MOF, Cu-ATC (also known as MOF-11), as first demonstrated by Chen *et al.* in 2000 (Fig. 1(c)).[26] This MOF exhibits a platinum sulfide (PtS) topology,[27] where each admantane unit is bound to four $Cu_2O_4C_8$ squares. Experimental N_2 adsorption measurements at 77 K have shown that Cu-ATC exhibits a low surface area and pore volume.[26,28]

Prior to 2019, ref. 26 reports the only experimental study on Cu-ATC when the MOF was first synthesized and published. In addition, to the best of our knowledge, the only theoretical study that was performed in Cu-ATC before 2019 was done by Choomwattana *et al.*, where the authors investigated using the MOF to encapsulate formaldehyde and propylene.[29] Previous experimental and theoretical studies have shown that Cu-ATC displays promising potential for various gas adsorption and separation applications.[28,30–32]

In 2019, it was observed that the presence of oppositely adjacent copper paddlewheels in the structure of Cu-ATC facilitated the trapping of a CH_4 molecule between two neighboring Cu^{2+} ions, which resulted in a high initial CH_4 Q_{st} value (26.8 kJ mol^{-1}).[28] Significant adsorption of CH_4 was also observed within the cavities of the aliphatic hydrocarbons of the alkylated ligand. In addition to having high CH_4 uptake, Cu-ATC displayed poor N_2 uptake, making it an excellent candidate for the extraction of CH_4 from coal-mine methane (a mixture that contains mostly N_2 and less than 50% CH_4).

In 2021, it was found that Cu-ATC had great ability to selectively adsorb C_2H_2 over CO_2 because of the extremely strong binding site between the two neighboring copper paddlewheels.[30] The equimolar C_2H_2/CO_2 selectivity for Cu-ATC at 298 K and 1 atm (53.6) is currently the highest out of all MOFs reported so far under this condition. Moreover, the initial Q_{st} value for C_2H_2 in this MOF was measured to be 79.1 kJ mol^{-1}, which is higher than that for other benchmark materials for C_2H_2 adsorption.

The self-adjusting nature of Cu-ATC and its ability to capture trace amounts of Xe and Kr from nuclear reprocessing off-gas was recently demonstrated.[31] Specifically, experimental studies have shown that Cu-ATC remained in a rigid conformation when exposed to N_2 and O_2, but shrinks and stretches its two main cavities to support the binding of Xe and Kr. This self-adjusting nature of Cu-ATC, paired with multiple weak binding interactions within the MOF, allows Xe and Kr to be selectively adsorbed over N_2 and O_2 within the hydrogen-rich cavities formed from the alkylated ligands.

It is expected that the affinity for H_2 in Cu-ATC would be high at low loading because of the presence of small pores within the material. Further, the distance between the Cu^{2+} ions of adjacent paddlewheels was measured to be 5.98 Å based on the dehydrated structure of the MOF.[26] This distance is short enough to suggest that a H_2 molecule can interact with the two Cu^{2+} ions concurrently, much like other gases did.[28,30,31] This should result in a high initial H_2 Q_{st} for this MOF, especially compared to that of Cu-BTC, which exhibits larger pore sizes. We attempt to verify these properties by carrying out experimental H_2 adsorption measurements in Cu-ATC, which are presented for the first time herein.

In this work, we performed grand canonical Monte Carlo (GCMC) simulations of H_2 adsorption in Cu-ATC and Cu-BTC. Due to the different pore sizes (arising from the different topology) of the respective materials, this study aims to investigate the effects of pore size on H_2 adsorption in these two MOFs that contain copper paddlewheel units. GCMC studies can provide detailed atomistic insights into the H_2 adsorption mechanisms in MOFs.[33] The locations of different binding sites in a MOF can be identified from GCMC simulations. In addition, simulated adsorption isotherms and Q_{st} values can be generated using this method, which can be directly compared to the experimental values.

We also carried out INS studies of H_2 adsorbed in both Cu-ATC and Cu-BTC. A molecular-level understanding of the H_2 adsorption affinity in both MOFs was obtained from the resulting INS spectra of the respective materials. Specifically, a comparison of the rotational tunneling transitions for the H_2–Cu^{2+} interaction in both Cu-ATC and Cu-BTC was gathered. The combination of INS studies, GCMC simulations, and quantum dynamics calculations can yield insights into the different H_2 adsorption sites and energetics in these two MOFs. The INS spectra of both MOFs contain a number of distinct peaks which mostly correspond to different binding sites in the MOFs. Assignment of these peaks can be achieved with the aid of two-dimensional quantum rotation calculations, where the rotational energy levels for each site can be obtained by solving the two-dimensional rigid rotor Hamiltonian with a theoretical potential energy surface for the respective sites.[18,34–42] In this work, we performed quantum rotation calculations for various H_2 binding sites in Cu-ATC and Cu-BTC. It will be shown that our calculated energy levels for the lowest transition (*i.e.*, the 0 to 1 transition) for each site considered in both MOFs is in good agreement with a certain peak in the corresponding spectra, which in turn led to a thorough interpretation of the INS spectra for the respective MOFs.

2. Methods

2.1 Experimental section

H_4ATC was synthesized according to previously reported methods.[43,44] Cu-ATC was synthesized and activated according to the procedures reported in ref. 26 and 30, with more details being provided in the ESI.† Phase purity of samples and evidence for the removal of coordinated H_2O molecules prior to gas adsorption measurements have been verified by performing powder X-ray diffraction (PXRD) analysis (see ESI, Fig. S5†).

The experimental H_2 adsorption isotherms for Cu-ATC at 77 and 87 K and pressures up to 1 atm were collected using

a Micromeritics ASAP 2020 surface area and porosity analyzer. Pore size distribution analysis based on N_2 adsorption measurements at 77 K using the same instrument confirms that the MOF exhibits small pore sizes (see ESI, Fig. S7†). The H_2 Q_{st} values were determined for a range of uptakes by applying the virial method[45,46] to the experimental isotherms at both temperatures (see ESI† for details). All experimental H_2 adsorption data displayed for Cu-BTC in this work were estimated from ref. 8.

The INS spectra for Cu-ATC and Cu-BTC were collected at a temperature of 10 K on the Quasi-Elastic Neutron Scattering (QENS) spectrometer at the Intense Pulsed Neutron Source (IPNS) of Argonne National Laboratory (ANL) using *ca.* 0.3 and 1.0 g of the activated sample, respectively. Successful loading of the material with amounts of H_2 related to the number of Cu in the sample was carried out *in situ* at 77 K after first obtaining a spectrum of the "blank" sample. The sample was equilibrated after loading before cooling to the data collection temperature of 10 K. The spectra shown for both MOFs in this work were obtained by subtracting the "blank" spectrum.

2.2 Theoretical section

The crystal structures used for the parameterizations and simulations in Cu-ATC and Cu-BTC herein were taken from ref. 26 and 11, respectively (refcodes BIMDIL and FIQCEN from the Cambridge Structure Database (CSD)[47]). Further, the dehydrated crystal structure of Cu-ATC was used in this study, since it was shown experimentally that the MOF was rigid and stable after the removal of all guest water molecules through thermal gravimetric analysis (TGA) and gas adsorption measurements.[26,28,30,31] All atoms in Cu-ATC and Cu-BTC were parameterized using repulsion/dispersion parameters, partial charges, and point polarizabilities to model van der Waals, electrostatic, and polarization interactions, respectively. The repulsion/dispersion parameters were taken from known general purpose force fields (*e.g.*, UFF,[48] OPLS-AA[49]). The Lennard-Jones 12-6 potential[50] was used to estimate van der Waals interactions.

The partial charges for the chemically distinct atoms in both MOFs (Fig. 2) were determined from electronic structure calculations on several fragments that were extracted from the crystal structure of the respective MOFs. Fragments in both MOFs were selected such that each chemically distinct atom was present in at least three fragments in which their chemical environments were similar to that of the MOF. The *ab initio* software package, NWChem,[51] was employed for these calculations. For all C, H, and O atoms, the 6-31G* basis set[52–54] was used, while the LANL2DZ ECP basis set[55–57] was used for the Cu^{2+} ions. For the fragments considered, the electrostatic potential surface was calculated using *ab initio* methods and the charges were fitted onto the atomic centers, using the CHELPG method,[58,59] to reproduce the surface. The partial charges for each chemically distinct atom were averaged between the fragments. Any atoms located near the fragment boundaries were discarded from consideration. Representational fragments for both Cu-ATC and Cu-BTC can be found in the ESI (Fig. S2 and S4†). The final calculated partial charges used in this work for both Cu-ATC and Cu-BTC can be found in Table 1. Note, the partial charges calculated herein for Cu-BTC are similar to those that were reported in previous work.[60–62]

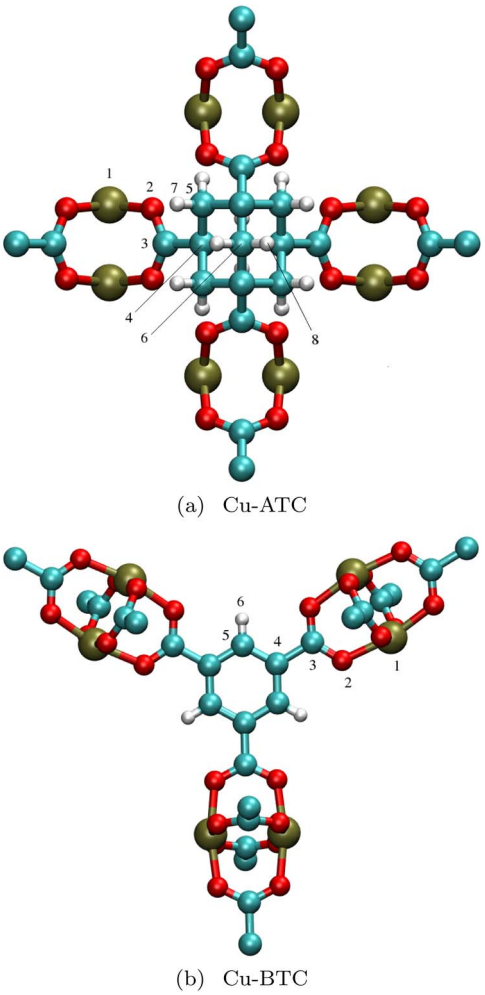

Fig. 2 The numbering of the chemically distinct atoms in (a) Cu-ATC and (b) Cu-BTC as referred to in Table 1. Atom colors: C = cyan, H = white, O = red, Cu = tan.

Electrostatic interactions were calculated by performing full Ewald summation.[63,64] Polarization interactions were calculated explicitly using a Thole-Applequist type model,[65–68] which has

Table 1 The partial charges (e^-) for the chemically distinct atoms in Cu-ATC and Cu-BTC. Label of atoms correspond to Fig. 2(a) and (b), respectively

Atom	Label	Cu-ATC q (e^-)	Atom	Label	Cu-BTC q (e^-)
Cu	1	1.16966	Cu	1	1.08076
O	2	−0.77336	O	2	−0.72538
C	3	0.86611	C	3	0.93474
C	4	0.22646	C	4	−0.21244
C	5	−0.16863	C	5	0.00951
C	6	−0.08184	H	6	0.17857
H	7	0.03437			
H	8	0.01013			

been executed consistently and successfully by our group.[36,37,39–42,69–71] The polarizabilities for all C, H, and O atoms were taken from van Duijnen *et al.*,[72] a carefully parametrized set that has been shown to be transferable, whereas the polarizability for Cu^{2+} was determined in previous work[70] and used herein.

Simulations of H_2 adsorption in both MOFs were performed using GCMC methods[73,74] with the Massively Parallel Monte Carlo (MPMC) code.[75,76] For Cu-ATC, the simulations were performed in the 3 × 3 × 2 supercell of the MOF as shown in Fig. 1(c). For Cu-BTC, a single unit cell of the MOF as shown in Fig. 1(d) was used for the simulations in this work. A spherical cut-off distance of 12.7010 and 13.1715 Å were utilized for Cu-ATC and Cu-BTC, respectively; these values correspond to half the shortest supercell/unit cell dimension length. For the temperatures considered in this work (77 and 87 K), quantum corrections were included in the simulations using the Feynman–Hibbs potential to the fourth order.[77] GCMC simulations at each state point considered consisted of 5.0×10^6 MC steps to guarantee equilibration, followed by an additional 5.0×10^6 steps to ensure reasonable ensemble averages for the total potential energy and particle number within the MOF–H_2 system. H_2 adsorption in both MOFs was simulated using a five-site polarizable potential that was developed by Belof *et al.*[78] Thus, all classical modeling results described herein are based on simulations that employed polarizable force fields. Control simulations were also performed using a single-site van der Waals model[79] and a five-site electrostatic model,[78] and the isotherms that were obtained using these models in both MOFs are presented in the ESI (Fig. S12 and S13†). The two-dimensional quantum rotation calculations were performed for each adsorption site considered in both MOFs by diagonalizing the rigid rotor Hamiltonian for the MOF–H_2 system as explained in previous work[35–42,80–86] and further described in the ESI.†

3. Results and discussion

3.1 Adsorption isotherms and isosteric heats of adsorption

A comparison of the experimental and simulated H_2 adsorption isotherms in Cu-ATC and Cu-BTC at 77 and 87 K and pressures up to 1 atm is shown in Fig. 3. The experimental data for Cu-BTC were estimated from ref. 8, while that for Cu-ATC are newly reported in this work. The relevant experimental properties and H_2 adsorption data for both MOFs are summarized in Table 2. Rowsell *et al.* found that the H_2 uptake for Cu-BTC at 77 K and 1 atm was about 2.60 wt%, which is higher than that for many MOFs that have been evaluated for H_2 storage under the same conditions.[2,20] Note, wt% is defined herein as: [(mass of H_2)/(mass of MOF + mass of H_2)] × 100%. The fact that Cu-BTC has a moderate surface area and contains open-metal sites probably contributes to the high H_2 uptake for this material at 77 K and 1 atm.

The experimental H_2 adsorption isotherms for Cu-ATC at 77 and 87 K display a significant sharp increase in uptake at pressures below 0.1 atm (Fig. 3). Indeed, at 77 K and 0.01 atm, the H_2 uptake for Cu-ATC is about 0.64 wt%, while that for Cu-BTC at the same state point is approximately 0.20 wt%. The higher H_2 uptake exhibited by Cu-ATC at low pressures (<0.1 atm) compared to Cu-BTC may be attributed to the presence of smaller pore sizes for the former. It has been previously demonstrated that smaller pore sizes in MOFs make it possible for the H_2 molecules to interact with multiple components of the framework simultaneously, which results in stronger MOF–H_2 interactions and greater adsorption of H_2 in the material.[38,87,88] Despite the high H_2 uptake for Cu-ATC at low pressures, the experimental isotherms at both 77 and 87 K for this MOF levels off at pressures beyond 0.2 atm. This indicates that the material quickly approaches H_2 saturation, a consequence of its low surface area. The experimental H_2 uptake for Cu-ATC at 77 K and 1 atm is only about 1.50 wt%. We note that the experimental isotherms shown for Cu-ATC at 77 and 87 K in Fig. 3 are reversible as the desorption curves at these temperatures are very similar to that for the corresponding adsorption curves (see ESI, Fig. S11†).

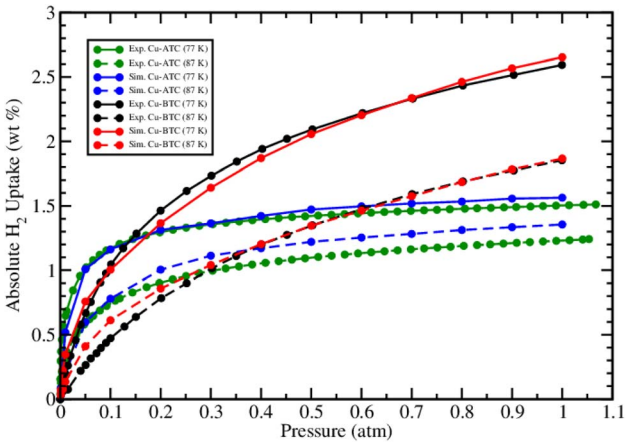

Fig. 3 Absolute H_2 adsorption isotherms for Cu-ATC (experiment = green, simulation = blue) and Cu-BTC (experiment = black, simulation = red) at 77 K (solid) and 87 K (dashed) and pressures up to 1 atm. The experimental data for Cu-BTC were estimated from ref. 8.

GCMC simulations in both MOFs using a polarizable H_2 potential produced isotherms that are in excellent agreement with the corresponding experimental isotherms across the

Table 2 Summary of the experimental properties and H_2 adsorption data for Cu-ATC and Cu-BTC. The Langmuir and BET surface areas and pore volume for Cu-ATC and Cu-BTC were taken from ref. 30 and 8, respectively. The experimental H_2 adsorption data for Cu-BTC were estimated from ref. 8

MOF	Cu-ATC	Cu-BTC
Langmuir surface area ($m^2\ g^{-1}$)	667	2175
BET surface area ($m^2\ g^{-1}$)	600	1507
Pore volume ($cm^3\ g^{-1}$)	0.23	0.75
H_2 uptake at 77 K/0.01 atm (wt%)	0.64	0.20
H_2 uptake at 77 K/1 atm (wt%)	1.50	2.60
H_2 uptake at 87 K/0.01 atm (wt%)	0.33	0.07
H_2 uptake at 87 K/1 atm (wt%)	1.23	1.85
Initial H_2 Q_{st} (kJ mol^{-1})	12.63	6.76

considered pressure range (Fig. 3). The simulated H_2 uptake for Cu-ATC and Cu-BTC at 77 K and 1 atm are 1.56 and 2.65 wt%, respectively, which are very close to the corresponding experimental values. The simulations also reproduced the same overall shape that is displayed by the experimental isotherms for both MOFs, suggesting proper modeling of the H_2 adsorption mechanism in these materials. The fact that the simulations yielded uptakes that are in close agreement with experiment at all state points considered for both MOFs engenders confidence in molecular-level predictions obtained from the theoretical studies, such as the preferred H_2 binding sites in these materials.

The experimental Q_{st} values for H_2 in Cu-ATC and Cu-BTC are displayed in Fig. 4. As with the adsorption isotherms, the H_2 Q_{st} values for Cu-ATC are presented for the first time in this work, while those for Cu-BTC were estimated from ref. 8. The experimental Q_{st} plots for both MOFs were obtained using the virial method.[45,46] According to the analysis performed by Rowsell *et al.*, the initial H_2 Q_{st} value for Cu-BTC is 6.76 kJ mol^{-1},[8] which is within a range that is typical for the binding of H_2 onto a single Cu^{2+} ion of a copper paddlewhel (6.0 to 7.0 kJ mol^{-1}).[2] This initial Q_{st} value is also consistent with the corresponding value reported in other experimental H_2 adsorption studies on the same MOF.[5–7] It can be observed that the Q_{st} for H_2 in Cu-BTC slightly decreases as the uptake increases, indicating that the H_2 molecules adsorb at slightly weaker binding sites in the material at higher loadings.

Virial analysis on the experimental H_2 adsorption isotherms for Cu-ATC reveals that the material exhibits a surprisingly high zero-loading H_2 Q_{st} of 12.63 kJ mol^{-1} (Fig. 4). To the best of our knowledge, this initial H_2 Q_{st} value for Cu-ATC is the highest out of all MOFs that contains copper paddlewheel units as it surpasses that for NOTT-201 (10.10 kJ mol^{-1}),[89] SNU-5 (11.60 kJ mol^{-1}),[90] and NOTT-209 (12.04 kJ mol^{-1}).[91] It is also greater than that for certain members of the M-MOF-74 series, such as Co-MOF-74 (11.9 kJ mol^{-1}) and Mg-MOF-74 (11.4 kJ mol^{-1}), and is only slightly lower than the corresponding value for Ni-MOF-74 (13.0 kJ mol^{-1}).[15] From a mathematical standpoint, the high initial H_2 Q_{st} value that was calculated for Cu-ATC from virial analysis can probably be attributed to the similarities in the shapes of the experimental isotherms at 77 and 87 K.

After initial loading, it can be observed that the Q_{st} for H_2 in Cu-ATC decreases to about 10 kJ mol^{-1} at *ca.* 3.7 mmol g^{-1} loading, after which the Q_{st} increases. The increase in Q_{st} with increasing loading beyond this point could be attributed to favorable H_2–H_2 interactions within the MOF at higher pressures, which is possible due to the small pore sizes of the material. Indeed, as the loading increases within the narrow pores of Cu-ATC, the H_2 molecules become closely packed within a confined space, which gives them the potential to interact favorably with both the MOF and each another. A similar behavior was observed in the Q_{st} plot for other gases in this MOF.[30,32]

Despite a high initial Q_{st} value, the H_2 adsorption process in Cu-ATC is reversible (*i.e.*, governed by physisorption) as suggested by the similarities in the adsorption and desorption isotherms for the adsorbate at 77 and 87 K (see ESI, Fig. S11†). In addition, we performed cycling experiments for H_2 adsorption in Cu-ATC at 77 K to evaluate the cycling performance and regenerability of this MOF. Details for performing these experiments are provided in the ESI.† After the first low-pressure adsorption cycle on a sample of activated Cu-ATC, H_2 adsorption was repeated on the same sample without the degassing process to obtain a second adsorption isotherm. The adsorption and desorption data for the first and second cycles are very similar to each other (see ESI, Fig. S9†), which indicates that Cu-ATC exhibits excellent regenerability upon H_2 adsorption. This MOF has also been demonstrated to display remarkable cycling performance for other gases.[28,31]

As explained in the next subsection, the primary binding site for H_2 in Cu-ATC corresponds to the adsorption of H_2 between two Cu^{2+} ions of adjacent copper paddlewheels. This site is associated with the high initial Q_{st} value for H_2 in the material. Indeed, as a H_2 molecule is adsorbed onto the Cu^{2+} ion of one copper paddlewheel, it can also interact with the Cu^{2+} ion of the nearby paddlewheel due to the short Cu^{2+}–Cu^{2+} distance between neighboring paddlewheels (5.98 Å). This results in a strong, synergistic interaction between the MOF and the H_2. The high initial H_2 Q_{st} value that was determined for Cu-ATC has been supported through periodic density functional theory (DFT) calculations for H_2 localized at the site between the two copper paddlewheels. Details of executing these calculations are provided in the ESI.† The adsorption energy for H_2 adsorbed between the two Cu^{2+} ions of adjacent copper paddlewheels in Cu-ATC was calculated to be −17.01 kJ mol^{-1}, which is comparable in magnitude to the zero-loading H_2 Q_{st} value for this MOF. As the loading increases, the H_2 Q_{st} for Cu-ATC decreases significantly beyond its initial loading value (Fig. 4), which implies that the subsequent H_2 adsorption sites in this MOF are notably weaker compared to binding between two neighboring Cu^{2+} ions.

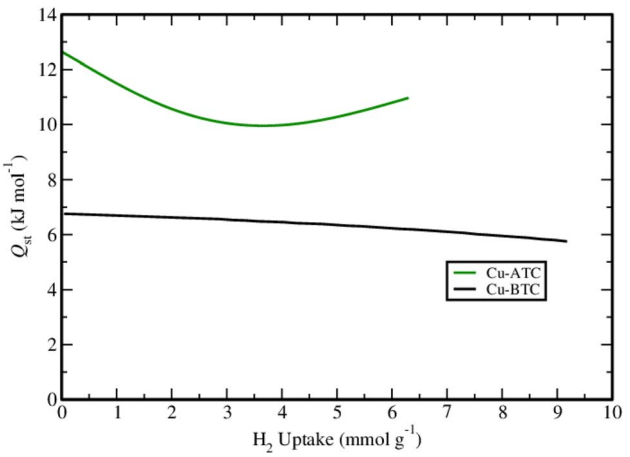

Fig. 4 Experimental isosteric heat of adsorption (Q_{st}) plotted against H_2 uptakes in Cu-ATC (green) and Cu-BTC (black). The experimental data for Cu-BTC was estimated from ref. 8.

3.2 Inelastic neutron scattering spectra, adsorption sites, and quantum rotation calculations

Detailed insights into the binding of H_2 in Cu-ATC and Cu-BTC at the microscopic level were gained by performing INS studies in both MOFs. The INS spectra for both MOFs are shown in Fig. 5 for loadings of 1, 2, and 3 H_2 molecules per Cu^{2+} ion sites. The INS spectra reveal prominent peaks at approximately 7.5 and 8.9 meV for Cu-ATC and Cu-BTC, respectively. These are the lowest energy peaks that are observed in the corresponding spectra for both MOFs, which implies high barriers to rotation and hence, strong interactions with the MOF for a particular adsorption site in both structures. These peaks correspond to the adsorption of H_2 onto the Cu^{2+} ions of the copper paddlewheels in the respective MOFs. This is consistent with observations in the INS spectra for other MOFs containing copper paddlewheels, such as PCN-12 (ref. 92) and rht-MOF-4a (ref. 93).

The fact that the lowest transition in Cu-ATC is located at an energy less than that in Cu-BTC suggests that the H_2–Cu^{2+} interaction is stronger in the former. This could be due to a number of reasons, with the foremost being the difference in the pore sizes between the two MOFs. The copper paddlewheels in Cu-ATC are aligned in such a way that two Cu^{2+} ions of adjacent paddlewheels are directly opposite to each other within the narrow channels (the Cu^{2+}–Cu^{2+} distance is 5.98 Å). When a H_2 molecule adsorbs onto a Cu^{2+} ion of a copper paddlewheel in Cu-ATC, it can also interact with the Cu^{2+} ion of the nearby paddlewheel, thus resulting in a favorable interaction. As a H_2 molecule is adsorbed onto a Cu^{2+} ion of a copper paddlewheel in Cu-BTC, there is no such synergistic interaction since the distance between the Cu^{2+} ions of two linearly aligned paddlewheels is about 16.0 Å.

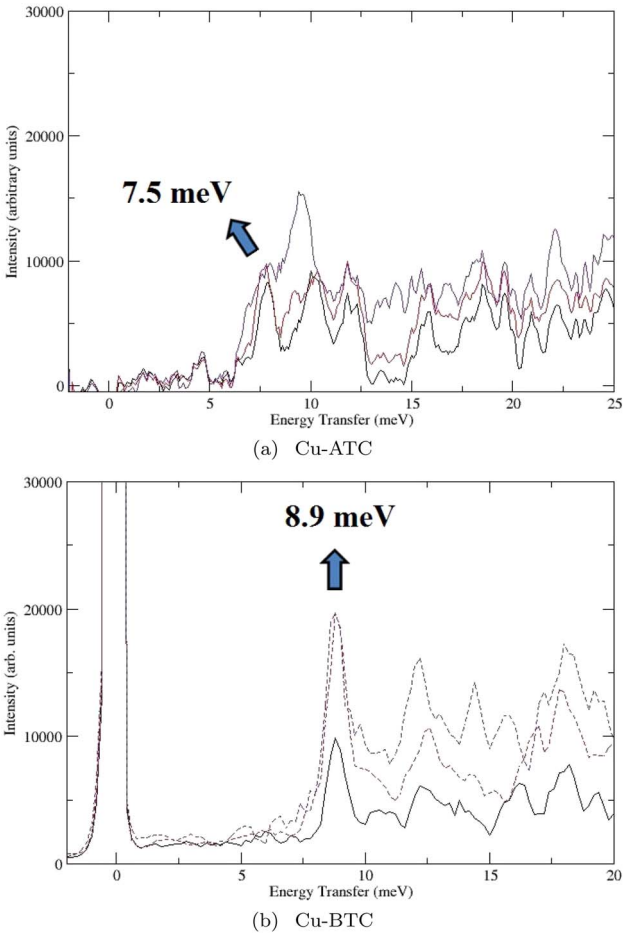

Fig. 5 Inelastic neutron scattering (INS) spectra for H_2 in (a) Cu-ATC and (b) Cu-BTC at different loadings: $1H_2$/Cu (black), $2H_2$/Cu (red), and $3H_2$/Cu (violet).

The difference in the calculated partial charges for the Cu^{2+} ions in Cu-ATC and Cu-BTC could also play a role for the different H_2–Cu^{2+} interaction between the two MOFs. As shown in Table 1, the partial charge of the Cu^{2+} ions is slightly more positive in Cu-ATC than in Cu-BTC (1.17 *vs.* $1.08e^-$). This suggests that the ATC ligands are more electron-rich, as it causes the coordinated Cu^{2+} ions in the MOF structure to exhibit a higher electropositivity. The higher electron deficiency of the Cu^{2+} ions in Cu-ATC implies that these ions can interact with the adsorbed H_2 molecules more strongly than the Cu^{2+} ions in Cu-BTC. It is also speculated that the H_2 molecules can approach the Cu^{2+} ions more closely in Cu-ATC since the removable aquo ligand is at a Cu^{2+}–O distance of 2.143 Å compared to 2.165 Å in Cu-BTC, thus leading to the larger rotational barrier for H_2 adsorbed in the former.

The adsorption of H_2 onto the Cu^{2+} ions in Cu-ATC and Cu-BTC was captured in the GCMC simulations performed in this work. As expected, the open-metal sites are the most favorable binding sites for H_2 in the respective MOFs. This was confirmed through analysis of the three-dimensional histograms showing the relative sites of H_2 occupancy in both MOFs as such histograms revealed that the H_2 molecules most frequently adsorb within the vicinity of the Cu^{2+} ions of the copper paddlewheels throughout the course of the GCMC simulations (see ESI, Fig. S14†). As explained above, and as shown in Fig. 6(a), the adsorbed H_2 molecule can make a favorable interaction with two Cu^{2+} ions of adjacent paddlewheels in Cu-ATC. Although the H_2 molecule is closer to one Cu^{2+} ion, the other Cu^{2+} ion is close enough to provide for a synergistic interaction. The Cu^{2+}–COM(H_2) distances were observed to be 2.46 and 3.56 Å, respectively. These distances are very close to those obtained through periodic DFT calculations that were carried out to optimize this H_2 molecule position in Cu-ATC (2.42 and 3.53 Å) (see ESI, Fig. S10(a)†). Note, a similar interaction has been observed in rht-MOF-7,[37] a MOF that exhibits rht topology.

The adsorption of H_2 onto a Cu^{2+} ion in Cu-BTC, as captured from the simulations, is depicted in Fig. 6(b). As mentioned above, the copper paddlewheels are much farther apart from each other in Cu-BTC; thus, a single H_2 molecule can only interact with one Cu^{2+} ion in this MOF, resulting in a weaker interaction compared to what was observed in Cu-ATC. For the simulations in this work, a Cu^{2+}–COM(H_2) distance of 2.50 Å was observed in Cu-BTC. This distance is in good agreement with the corresponding distances that were observed in Cu-BTC through neutron powder diffraction (2.39(1) Å)[94] and *ab initio* calculations (2.47 Å).[18] We also performed periodic DFT calculations to optimize the position of a H_2 molecule about a single Cu^{2+} ion of a copper paddlewheel in Cu-BTC using the same

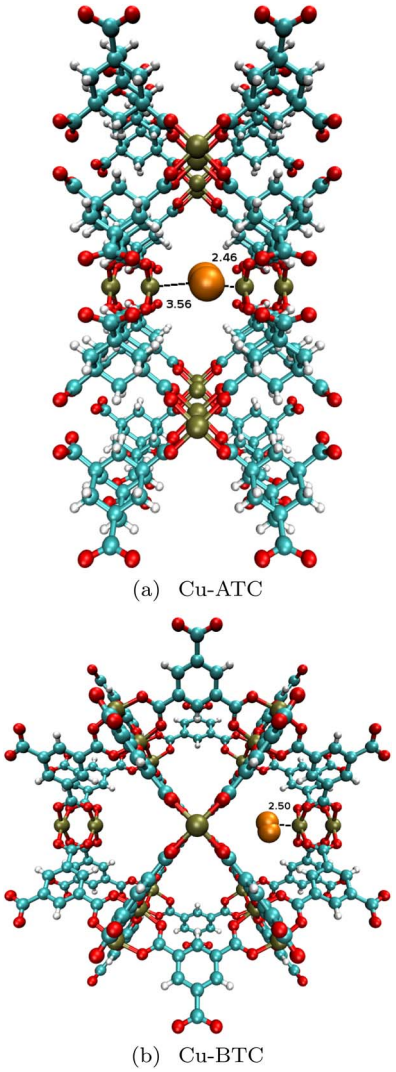

(a) Cu-ATC

(b) Cu-BTC

Fig. 6 A molecular illustration of the H_2 binding site (a) between the Cu^{2+} ions of adjacent copper paddlewheels in Cu-ATC and (b) about a single Cu^{2+} ion in Cu-BTC as determined from simulation. The adsorbate molecules are shown in orange. Atom colors: C = cyan, H = white, O = red, Cu = tan.

methods that were employed for Cu-ATC (see ESI, Fig. S10(b)†). The Cu^{2+}–COM(H_2) distance for this optimized position in Cu-BTC was measured to be 2.44 Å, which is in good agreement with the corresponding distance that was obtained through GCMC simulation. The calculated adsorption energy for this position is −12.23 kJ mol^{-1}, which is somewhat higher in magnitude than the initial H_2 Q_{st} for this MOF (6.76 kJ mol^{-1}), but still lower than the analogous adsorption energy that was calculated for H_2 adsorbed between two adjacent copper paddlewheels in Cu-ATC (−17.01 kJ mol^{-1}). We note that the magnitudes of the calculated adsorption energies for H_2 localized about the Cu^{2+} ion(s) in both MOFs are higher than the initial H_2 Q_{st} for the individual MOFs by similar values (*ca.* 4–5 kJ mol^{-1}).

The assignment of the 7.5 and 8.9 meV peaks in the INS spectra for Cu-ATC and Cu-BTC, respectively, as adsorption onto the Cu^{2+} ions in the respective MOFs is supported by the

Table 3 The calculated two-dimensional quantum rotational levels for a H_2 molecule adsorbed at the two sites in Cu-ATC. Sites 1, 2, 3, and 4 are depicted in Fig. 6(a), 7(a), 7(b), and 7(c), respectively. Relative energies are given in meV

n	j	Site 1 ΔE (meV)	Site 2 ΔE (meV)	Site 3 ΔE (meV)	Site 4 ΔE (meV)
1	0	0.00	0.00	0.00	0.00
2		7.75	10.77	12.43	9.81
3	1	9.24	16.05	15.22	15.90
4		33.14	18.51	16.84	20.50
5		33.38	41.74	42.51	41.06
6		57.93	41.99	42.77	41.23
7	2	72.91	43.88	43.95	44.51
8		74.25	47.68	45.99	48.93
9		75.05	48.03	46.19	49.80

two-dimensional quantum rotation calculations performed herein. The rotational energy levels for a H_2 molecule adsorbed about a Cu^{2+} ion in Cu-ATC and Cu-BTC are provided in Tables 3 and 4, respectively. We note that the entire system (*i.e.*, all atoms) for both MOFs was used for the calculations. For a H_2 molecule adsorbed about the Cu^{2+} ions in Cu-ATC, a 0 to 1 transition of 7.75 meV was calculated. This is in very good agreement with the 7.5 meV peak that is observed in the INS spectra for Cu-ATC. A rotational level of 9.07 meV was calculated as the lowest transition for a H_2 molecule adsorbed onto the Cu^{2+} ion in Cu-BTC. As with Cu-ATC, this is in very good agreement with the lowest energy peak that is observed in the INS spectra for Cu-BTC. Indeed, the quantum rotation calculations executed herein confirmed the assignments of the lowest energy peaks for both MOFs and verified that the H_2–Cu^{2+} interaction is stronger in Cu-ATC than in Cu-BTC. We note that the rotational levels for the H_2–Cu^{2+} interaction in Cu-BTC reported herein are similar to those that were calculated in the work of Brown *et al.*[18] In addition, quantum rotation calculations performed on the H_2 molecule positions that were obtained through DFT calculations in Cu-ATC and Cu-BTC produced rotational levels that are similar to those shown for the primary binding sites in Tables 3 and 4. Thus, the DFT calculations also support the assignment of the lowest energy peak in the INS spectra of both MOFs.

Table 4 The calculated two-dimensional quantum rotational levels for a H_2 molecule adsorbed at the two sites in Cu-BTC. Sites 1 and 2 are depicted in Fig. 6(b) and 8, respectively. Relative energies are given in meV

n	j	Site 1 ΔE (meV)	Site 2 ΔE (meV)
1	0	0.00	0.00
2		9.07	12.64
3	1	9.25	14.88
4		35.09	16.94
5		35.13	42.45
6		46.01	42.73
7	2	62.04	44.20
8		62.18	45.74
9		76.82	46.16

Additional peaks at higher energies can be seen in the INS spectra for both Cu-ATC and Cu-BTC. In Cu-BTC, there are three peaks at approximately 12.4, 14.0, and 16.0 meV which increase in intensity as the loading increases. All of these peaks could be attributed to the adsorption of H_2 at one particular binding site in the MOF (site 2). On the other hand, it can be observed that the INS spectra for Cu-ATC are more complex than those for Cu-BTC, as even at the lowest loading measured ($1H_2$/Cu), there are three peaks (occurring at approximately 7.5, 10.0, and 12.0 meV) with similar intensities. While the peak at 7.5 meV corresponds to the adsorption of H_2 onto the Cu^{2+} ions as explained above, the peaks at 10.0 and 12.0 meV could correspond to one or two similar adsorption sites in the MOF. The fact that these peaks have intensities that are similar to that for the 7.5 meV peak indicates that the sites corresponding to these peaks are being filled concurrently with the Cu^{2+} ion sites at low loading. In addition, at the highest loading measured ($3H_2$/Cu), there is huge peak at approximately 9.0 meV, which has no counterpart in Cu-BTC. The interpretation of these features in the INS spectra for both Cu-ATC and Cu-BTC was achieved through the two-dimensional quantum rotation calculations performed herein.

The simulations executed herein assisted in the identification of the additional H_2 adsorption sites in Cu-ATC as observed in the INS spectra for the MOF. It was discovered that the H_2 molecules prefer to crowd into the center of the channels in the MOF. Specifically, the H_2 molecules adsorb into a confined region that is surrounded by four neighboring copper paddlewheel units (Fig. 7(a)). This site was observed in the simulations even at low loadings due to the small pore sizes of the MOF and is consistent with the observations in the INS spectra. Calculation of the two-dimensional quantum rotational levels for a H_2 molecule adsorbed about this site in Cu-ATC revealed a 0 to 1 transition of 10.77 meV (Table 3). This value is in good agreement with the peak that is observed at approximately 10.0 meV in the INS spectra for the MOF. Since the aforementioned site is a common adsorption site in the MOF and has relatively weaker energetics than the Cu^{2+} ion sites, we have assigned the 10.0 meV peak to this site based on the agreement between the experimental and calculated rotational transitions.

The simulations revealed that the H_2 molecules also prefer to adsorb into the upper and lower portions of the channels in Cu-ATC (Fig. 7(b)). In this region, the H_2 molecules can interact with the enclosing ATC ligands in the structure. Like the previous adsorption site, this site was observed from the simulations at low loadings due to the presence of the narrow pores. The energetics associated with this site is weaker than that of the previous site; thus, the rotational transition for this site should be found at higher energies in the INS spectra. It is predicted that this site corresponds to the peak at approximately 12.0 meV in the spectra. Calculation of the two-dimensional quantum rotational levels for a H_2 molecule adsorbed at this site has verified this assumption, as a rotational level of 12.43 meV was calculated for the lowest transition (Table 3).

Insights into the reason for the noticeable large peak at about 9.0 meV at the highest loading measured in the INS spectra for Cu-ATC were gained from the simulations in the MOF at higher loadings. At higher loadings, it was observed that the H_2 molecules essentially pack into the center of the channels as depicted in Fig. 7(a). However, as more H_2 molecules enter, they are forced to be closer to the sides of this region and

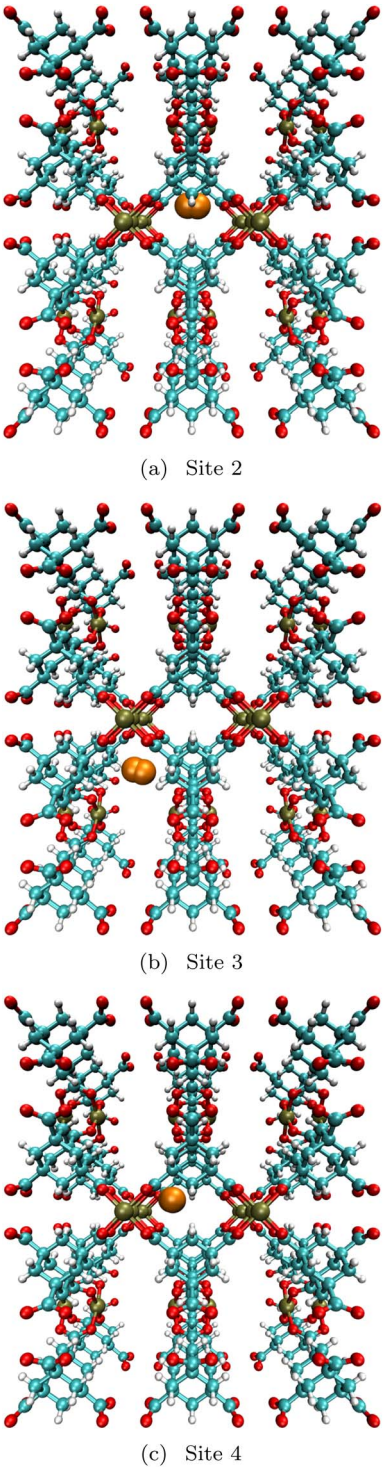

Fig. 7 A molecular illustration of the H_2 binding site about sites 2, 3, and 4 in Cu-ATC as determined from simulation. The adsorbate molecules are shown in orange. Atom colors: C = cyan, H = white, O = red, Cu = tan.

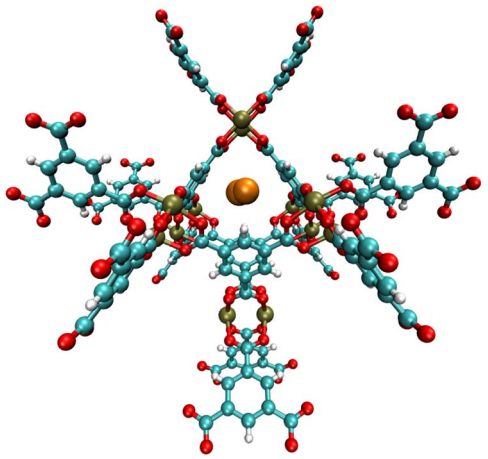

Fig. 8 A molecular illustration of the H_2 binding site within the tetrahedral cage in Cu-BTC as determined from simulation. The adsorbate molecule is shown in orange. Atom colors: C = cyan, H = white, O = red, Cu = tan.

near the copper paddlewheels (Fig. 7(c)). We have therefore identified this site as a distinct adsorption site in Cu-ATC. Since these H_2 molecules are adsorbed in the proximity of the paddlewheels, the rotational level for the lowest transition for this site should be slightly reduced compared to that for a H_2 molecule adsorbed at the center of the channel. Indeed, a 0 to 1 transition of 9.81 meV was calculated for the site shown in Fig. 7(c), which is in good agreement with the 9.0 meV peak (Table 3). Thus, we believe that the noticeable large peak at about 9.0 meV at a loading of $3H_2$/Cu represents an enlargement and shifting (to lower energies) of the 10.0 meV peak that is seen at lower loadings. Additional peaks can be observed beyond the rigid rotor limit (14.7 meV) in the INS spectra for Cu-ATC. These peaks agree well with the calculated second or third transitions for the three previously described sites (Table 3).

It was observed in the simulations that the secondary adsorption sites in Cu-BTC corresponded to the adsorption of H_2 into the tetrahedral cages in the MOF; a molecular illustration of this adsorption site is shown in Fig. 8. Calculation of the rotational energy levels for a H_2 molecule adsorbed at this site in Cu-BTC resulted in values of 12.64, 14.88, and 16.94 meV for the $j = 1$ level (Table 4). These values are in very good agreement with the peaks that are observed at approximately 12.4, 14.0, and 16.0 meV, respectively, in the INS spectra for Cu-BTC. As a result, the assignment of these peaks have been made to the aforementioned site. This confirms that these three peaks are attributed to the adsorption of H_2 at one particular binding site in the MOF. After the Cu^{2+} ion sites are filled in Cu-BTC, the H_2 molecules essentially crowd into the tetrahedral cages in the MOF. This has been observed as an adsorption site in Cu-BTC through neutron powder diffraction studies.[94,95]

4. Conclusion

Experimental H_2 adsorption data for Cu-ATC was presented for the first time and such results were compared with those for the well-known Cu-BTC. It was found that Cu-ATC displays higher H_2 uptake than Cu-BTC at low pressures (<0.1 atm) due to possessing smaller pore sizes. However, the low surface area of Cu-ATC limits the H_2 adsorption capacity in this material at higher pressures. We also describe the results of theoretical studies of H_2 adsorbed in Cu-ATC and Cu-BTC. Notably, GCMC simulations generated H_2 adsorption isotherms that are in outstanding agreement with the corresponding experimental data for both MOFs.

The simulations confirmed that the exposed Cu^{2+} ions of the copper paddlewheels represent the primary binding site for H_2 in both MOFs. However, the short Cu^{2+}–Cu^{2+} distance between adjacent copper paddlewheels in Cu-ATC (5.98 Å) allows a H_2 molecule to interact with these two neighboring Cu^{2+} ions simultaneously. The binding of H_2 between these two adjacent Cu^{2+} ions gives rise to a surprisingly high initial H_2 Q_{st} value for the material. Particularly, this value for Cu-ATC (12.63 kJ mol^{-1}) is among the highest of MOFs that have been reported in the literature.[2,20] Periodic DFT calculations for a H_2 molecule adsorbed at this site produced an adsorption energy that is comparable in magnitude to the aforementioned initial Q_{st}. On the other hand, a H_2 molecule can only interact with a single Cu^{2+} ion when it is adsorbed about a copper paddlewheel in Cu-BTC. As a result, the H_2–Cu^{2+} interaction in this MOF is weaker compared to that in Cu-ATC, with a much lower zero-loading Q_{st} value for H_2.

The INS spectra for H_2 adsorbed in both MOFs were also presented and revealed prominent low energy transfer peaks occurring at approximately 7.5 and 8.9 meV for Cu-ATC and Cu-BTC, respectively. These peaks correspond to the adsorption of H_2 onto the Cu^{2+} ions of the copper paddlewheels in the respective MOFs. The fact that the lowest energy peak was found at lower energies (which implies smaller tunnel splitting) in Cu-ATC implies that the barrier to rotation for H_2 adsorbed onto the Cu^{2+} ions is higher in Cu-ATC than in Cu-BTC, thus signifying that the H_2–Cu^{2+} interaction is stronger in the former. These results have been validated through calculation of the two-dimensional quantum rotational levels. Further, comprehensive interpretations of the INS spectra for both MOFs have been accomplished through the aid of such calculations.

It was shown herein that Cu-ATC is an impressive material that exhibits high H_2 uptake at low pressures and a high Q_{st} value for H_2 at zero-coverage. The exceptional H_2 adsorption characteristics for this MOF is attributed to the presence of oppositely adjacent copper paddlewheels, which allows for a H_2 molecule to interact with two neighboring Cu^{2+} ions simultaneously. It is expected that the adsorption energetics for a H_2 molecule about this site can be increased further if the distance between the adjacent copper paddlewheels is reduced or if polar functionalities are introduced onto the adamantane units. The effects of such modifications on H_2 adsorption could potentially be investigated in future experimental and/or theoretical studies.

Conflicts of interest

The authors declare no competing financial interest.

Acknowledgements

T. P., K. A. F., B. T., and B. S. acknowledge the National Science Foundation (Award No. DMR-1607989), including support from the Major Research Instrumentation Program (Award No. CHE-1531590). Computational resources were made available by an ACCESS Grant (No. TG-DMR090028), Research Computing at the University of South Florida, and High-Performance Computing at North Carolina State University. S. M. acknowledges partial support from the Hydrogen and Fuel Cell Technologies and Vehicle Technologies Office within the U.S. Department of Energy's Office of Energy Efficiency and Renewable Energy (Award No. DE-EE0008810). We thank Professor Rahul Banerjee for preparing a sample of Cu-BTC and his assistance with data collection at IPNS.

References

1 D. Zhao, D. Yuan and H.-C. Zhou, *Energy Environ. Sci.*, 2008, **1**, 222–235.
2 M. P. Suh, H. J. Park, T. K. Prasad and D.-W. Lim, *Chem. Rev.*, 2012, **112**, 782–835.
3 S. K. Bhatia and A. L. Myers, *Langmuir*, 2006, **22**, 1688–1700.
4 Y.-S. Bae and R. Q. Snurr, *Microporous Mesoporous Mater.*, 2010, **132**, 300–303.
5 J. Lee, J. Li and J. Jagiello, *J. Solid State Chem.*, 2005, **178**, 2527–2532.
6 P. Krawiec, M. Kramer, M. Sabo, R. Kunschke, H. Fröde and S. Kaskel, *Adv. Eng. Mater.*, 2006, **8**, 293–296.
7 B. Panella, M. Hirscher, H. Pütter and U. Müller, *Adv. Funct. Mater.*, 2006, **16**, 520–524.
8 J. L. C. Rowsell and O. M. Yaghi, *J. Am. Chem. Soc.*, 2006, **128**, 1304–1315.
9 A. G. Wong-Foy, A. J. Matzger and O. M. Yaghi, *J. Am. Chem. Soc.*, 2006, **128**, 3494–3495.
10 B. Xiao, P. S. Wheatley, X. Zhao, A. J. Fletcher, S. Fox, A. G. Rossi, I. L. Megson, S. Bordiga, L. Regli, K. M. Thomas and R. E. Morris, *J. Am. Chem. Soc.*, 2007, **129**, 1203–1209.
11 S. S.-Y. Chui, S. M.-F. Lo, J. P. H. Charmant, A. G. Orpen and I. D. Williams, *Science*, 1999, **283**, 1148–1150.
12 N. L. Rosi, J. Eckert, M. Eddaoudi, D. T. Vodak, J. Kim, M. O'Keeffe and O. M. Yaghi, *Science*, 2003, **300**, 1127–1129.
13 J. L. C. Rowsell, J. Eckert and O. M. Yaghi, *J. Am. Chem. Soc.*, 2005, **127**, 14904–14910.
14 S. Ma, J. Eckert, P. M. Forster, J. W. Yoon, Y. K. Hwang, J.-S. Chang, C. D. Collier, J. B. Parise and H.-C. Zhou, *J. Am. Chem. Soc.*, 2008, **130**, 15896–15902.
15 P. D. C. Dietzel, P. A. Georgiev, J. Eckert, R. Blom, T. Strassle and T. Unruh, *Chem. Commun.*, 2010, **46**, 4962–4964.
16 J. Eckert and W. Lohstroh, in *Neutron Applications in Materials for Energy*, ed. G. J. Kearley and V. K. Peterson, Springer International Publishing, 2015, pp. 205–239.
17 T. Pham, K. A. Forrest, B. Space and J. Eckert, *Phys. Chem. Chem. Phys.*, 2016, **18**, 17141–17158.
18 C. M. Brown, Y. Liu, T. Yildirim, V. K. Peterson and C. J. Kepert, *Nanotechnology*, 2009, **20**, 204025.
19 J. P. Perdew, J. A. Chevary, S. H. Vosko, K. A. Jackson, M. R. Pederson, D. J. Singh and C. Fiolhais, *Phys. Rev. B: Condens. Matter Mater. Phys.*, 1992, **46**, 6671–6687.
20 Y. He, B. Li, M. O'Keeffe and B. Chen, *Chem. Soc. Rev.*, 2014, **43**, 5618–5656.
21 O. Ermer, *J. Am. Chem. Soc.*, 1988, **110**, 3747–3754.
22 X. Lin, I. Telepeni, A. J. Blake, A. Dailly, C. M. Brown, J. M. Simmons, M. Zoppi, G. S. Walker, K. M. Thomas, T. J. Mays, P. Hubberstey, N. R. Champness and M. Schröder, *J. Am. Chem. Soc.*, 2009, **131**, 2159–2171.
23 W.-Y. Gao, Y. Niu, Y. Chen, L. Wojtas, J. Cai, Y.-S. Chen and S. Ma, *CrystEngComm*, 2012, **14**, 6115–6117.
24 A. Gomila, S. Duval, C. Besnard, K. W. Krämer, S.-X. Liu, S. Decurtins and A. F. Williams, *Inorg. Chem.*, 2014, **53**, 2683–2691.
25 R.-J. Li, M. Li, X.-P. Zhou, D. Li and M. O'Keeffe, *Chem. Commun.*, 2014, **50**, 4047–4049.
26 B. Chen, M. Eddaoudi, T. M. Reineke, J. W. Kampf, M. O'Keeffe and O. M. Yaghi, *J. Am. Chem. Soc.*, 2000, **122**, 11559–11560.
27 V. A. Blatov, A. P. Shevchenko and V. N. Serezhkin, *J. Appl. Crystallogr.*, 2000, **33**, 1193.
28 Z. Niu, X. Cui, T. Pham, P. C. Lan, H. Xing, K. A. Forrest, L. Wojtas, B. Space and S. Ma, *Angew. Chem., Int. Ed.*, 2019, **58**, 10138–10141.
29 S. Choomwattana, T. Maihom, P. Khongpracha, M. Probst and J. Limtrakul, *J. Phys. Chem. C*, 2008, **112**, 10855–10861.
30 Z. Niu, X. Cui, T. Pham, G. Verma, P. C. Lan, C. Shan, H. Xing, K. A. Forrest, S. Suepaul, B. Space, A. Nafady, A. M. Al-Enizi and S. Ma, *Angew. Chem., Int. Ed.*, 2021, **60**, 5283–5288.
31 Z. Niu, Z. Fan, T. Pham, G. Verma, K. A. Forrest, B. Space, P. K. Thallapally, A. M. Al-Enizi and S. Ma, *Angew. Chem., Int. Ed.*, 2022, **61**, e202117807.
32 C. Zhang, X. Dong, Y. Chen, H. Wu, L. Yu, K. Zhou, Y. Wu, Q. Xia, H. Wang, Y. Han and J. Li, *Sep. Purif. Technol.*, 2022, **291**, 120932.
33 T. Pham and B. Space, *Top. Curr. Chem.*, 2020, **378**, 14.
34 L. Kong, G. Román-Pérez, J. M. Soler and D. C. Langreth, *Phys. Rev. Lett.*, 2009, **103**, 096103.
35 I. Matanović, J. L. Belof, B. Space, K. Sillar, J. Sauer, J. Eckert and Z. Bačić, *J. Chem. Phys.*, 2012, **137**, 014701.
36 T. Pham, K. A. Forrest, A. Hogan, K. McLaughlin, J. L. Belof, J. Eckert and B. Space, *J. Mater. Chem. A*, 2014, **2**, 2088–2100.
37 T. Pham, K. A. Forrest, J. Eckert, P. A. Georgiev, A. Mullen, R. Luebke, A. J. Cairns, Y. Belmabkhout, J. F. Eubank, K. McLaughlin, W. Lohstroh, M. Eddaoudi and B. Space, *J. Phys. Chem. C*, 2014, **118**, 439–456.
38 P. Nugent, T. Pham, K. McLaughlin, P. A. Georgiev, W. Lohstroh, J. P. Embs, M. J. Zaworotko, B. Space and J. Eckert, *J. Mater. Chem. A*, 2014, **2**, 13884–13891.
39 T. Pham, K. A. Forrest, K. McLaughlin, J. Eckert and B. Space, *J. Phys. Chem. C*, 2014, **118**, 22683–22690.
40 T. Pham, K. A. Forrest, P. A. Georgiev, W. Lohstroh, D.-X. Xue, A. Hogan, M. Eddaoudi, B. Space and J. Eckert, *Chem. Commun.*, 2014, **50**, 14109–14112.

41 T. Pham, K. A. Forrest, R. Banerjee, G. Orcajo, J. Eckert and B. Space, *J. Phys. Chem. C*, 2015, **119**, 1078–1090.
42 T. Pham, K. A. Forrest, A. Hogan, B. Tudor, K. McLaughlin, J. L. Belof, J. Eckert and B. Space, *Cryst. Growth Des.*, 2015, **15**, 1460–1471.
43 G. R. Newkome, A. Nayak, R. K. Behera, C. N. Moorefield and G. R. Baker, *J. Org. Chem.*, 1992, **57**, 358–362.
44 Q. Fang, S. Gu, J. Zheng, Z. Zhuang, S. Qiu and Y. Yan, *Angew. Chem., Int. Ed.*, 2014, **53**, 2878–2882.
45 L. Czepirski and J. JagieŁŁo, *Chem. Eng. Sci.*, 1989, **44**, 797–801.
46 M. Dincă, A. Dailly, Y. Liu, C. M. Brown, D. A. Neumann and J. R. Long, *J. Am. Chem. Soc.*, 2006, **128**, 16876–16883.
47 F. H. Allen, *Acta. Crystallogr., B.*, 2002, **58**, 380–388.
48 A. K. Rappé, C. J. Casewit, K. S. Colwell, W. A. Goddard and W. M. Skiff, *J. Am. Chem. Soc.*, 1992, **114**, 10024–10035.
49 W. L. Jorgensen, D. S. Maxwell and J. Tirado-Rives, *J. Am. Chem. Soc.*, 1996, **118**, 11225–11236.
50 J. E. Jones, *Proc. R. Soc. London, Ser. A*, 1924, **106**, 463–477.
51 M. Valiev, E. Bylaska, N. Govind, K. Kowalski, T. Straatsma, H. V. Dam, D. Wang, J. Nieplocha, E. Apra, T. Windus and W. de Jong, *Comput. Phys. Commun.*, 2010, **181**, 1477–1489.
52 R. Ditchfield, W. J. Hehre and J. A. Pople, *J. Chem. Phys.*, 1971, **54**, 724–728.
53 P. C. Hariharan and J. A. Pople, *Theor. Chim. Acta*, 1973, **28**, 213–222.
54 W. J. Hehre, R. Ditchfield and J. A. Pople, *J. Chem. Phys.*, 1972, **56**, 2257–2261.
55 W. J. Stevens, H. Basch and M. Krauss, *J. Chem. Phys.*, 1984, **81**, 6026–6033.
56 P. J. Hay and W. R. Wadt, *J. Chem. Phys.*, 1985, **82**, 270–283.
57 L. A. LaJohn, P. A. Christiansen, R. B. Ross, T. Atashroo and W. C. Ermler, *J. Chem. Phys.*, 1987, **87**, 2812–2824.
58 L. E. Chirlian and M. M. Francl, *J. Comput. Chem.*, 1987, **8**, 894–905.
59 C. M. Breneman and K. B. Wiberg, *J. Comput. Chem.*, 1990, **11**, 361–373.
60 Q. Yang and C. Zhong, *J. Phys. Chem. B*, 2006, **110**, 17776–17783.
61 A. O. Yazaydin, A. I. Benin, S. A. Faheem, P. Jakubczak, J. J. Low, R. R. Willis and R. Q. Snurr, *Chem. Mater.*, 2009, **21**, 1425–1430.
62 D.-L. Chen, A. C. Stern, B. Space and J. K. Johnson, *J. Phys. Chem. A*, 2010, **114**, 10225–10233.
63 P. P. Ewald, *Ann. Phys.*, 1921, **369**, 253–287.
64 B. A. Wells and A. L. Chaffee, *J. Chem. Theory Comput.*, 2015, **11**, 3684–3695.
65 J. Applequist, J. R. Carl and K.-K. Fung, *J. Am. Chem. Soc.*, 1972, **94**, 2952–2960.
66 B. Thole, *Chem. Phys.*, 1981, **59**, 341–350.
67 K. A. Bode and J. Applequist, *J. Phys. Chem.*, 1996, **100**, 17820–17824.
68 K. McLaughlin, C. R. Cioce, T. Pham, J. L. Belof and B. Space, *J. Chem. Phys.*, 2013, **139**, 184112.
69 J. L. Belof, A. C. Stern, M. Eddaoudi and B. Space, *J. Am. Chem. Soc.*, 2007, **129**, 15202–15210.
70 K. A. Forrest, T. Pham, K. McLaughlin, J. L. Belof, A. C. Stern, M. J. Zaworotko and B. Space, *J. Phys. Chem. C*, 2012, **116**, 15538–15549.
71 T. Pham, K. A. Forrest, P. Nugent, Y. Belmabkhout, R. Luebke, M. Eddaoudi, M. J. Zaworotko and B. Space, *J. Phys. Chem. C*, 2013, **117**, 9340–9354.
72 P. T. van Duijnen and M. Swart, *J. Phys. Chem. A*, 1998, **102**, 2399–2407.
73 N. Metropolis, A. W. Rosenbluth, M. N. Rosenbluth, A. H. Teller and E. Teller, *J. Chem. Phys.*, 1953, **21**, 1087–1092.
74 D. Frenkel and B. Smit, *Understanding Molecular Simulation: from Algorithms to Applications*, Academic Press, New York, 2002.
75 J. L. Belof and B. Space, *Massively Parallel Monte Carlo (MPMC)*, available on GitHub, 2012, **https://github.com/mpmccode/mpmc**.
76 D. M. Franz, J. L. Belof, K. McLaughlin, C. R. Cioce, B. Tudor, A. Hogan, L. Laratelli, M. Mulcair, M. Mostrom, A. Navas, A. C. Stern, K. A. Forrest, T. Pham and B. Space, *Adv. Theory Simul.*, 2019, **2**, 1900113.
77 R. P. Feynman and A. R. Hibbs, *Quantum Mechanics and Path Integrals*, McGraw-Hill, New York, 1965.
78 J. L. Belof, A. C. Stern and B. Space, *J. Chem. Theory Comput.*, 2008, **4**, 1332–1337.
79 V. Buch, *J. Chem. Phys.*, 1994, **100**, 7610–7629.
80 K. A. Forrest, T. Pham, P. A. Georgiev, J. P. Embs, N. W. Waggoner, A. Hogan, S. M. Humphrey, J. Eckert and B. Space, *Chem. Mater.*, 2015, **27**, 7619–7626.
81 T. Pham, K. A. Forrest, E. H. L. Falcão, J. Eckert and B. Space, *Phys. Chem. Chem. Phys.*, 2016, **18**, 1786–1796.
82 T. Pham, K. A. Forrest, J. Eckert and B. Space, *Cryst. Growth Des.*, 2016, **16**, 867–874.
83 T. Pham, K. A. Forrest, M. Mostrom, J. R. Hunt, H. Furukawa, J. Eckert and B. Space, *Phys. Chem. Chem. Phys.*, 2017, **19**, 13075–13082.
84 T. Pham, K. A. Forrest, H. Furukawa, M. Russina, A. Albinati, P. A. Georgiev, J. Eckert and B. Space, *J. Phys. Chem. C*, 2017, **121**, 1723–1733.
85 T. Pham, K. A. Forrest, H. Furukawa, J. Eckert and B. Space, *J. Phys. Chem. C*, 2018, **122**, 15435–15445.
86 S. Suepaul, K. A. Forrest, P. A. Georgiev, P. M. Forster, W. Lohstroh, V. Grzimek, S. G. Dunning, J. E. Reynolds, S. M. Humphrey, J. Eckert, B. Space and T. Pham, *ACS Appl. Mater. Interfaces*, 2022, **14**, 8126–8136.
87 B. Kesanli, Y. Cui, M. R. Smith, E. W. Bittner, B. C. Bockrath and W. Lin, *Angew. Chem., Int. Ed.*, 2005, **44**, 72–75.
88 S. Ma, D. Sun, M. Ambrogio, J. A. Fillinger, S. Parkin and H.-C. Zhou, *J. Am. Chem. Soc.*, 2007, **129**, 1858–1859.
89 S. Yang, X. Lin, A. J. Blake, G. S. Walker, P. Hubberstey, N. R. Champness and M. Schröder, *Nat. Chem.*, 2009, **1**, 487–493.
90 Y.-G. Lee, H. R. Moon, Y. E. Cheon and M. P. Suh, *Angew. Chem., Int. Ed.*, 2008, **47**, 7741–7745.
91 S. Yang, S. K. Callear, A. J. Ramirez-Cuesta, W. I. F. David, J. Sun, A. J. Blake, N. R. Champness and M. Schröder, *Faraday Discuss.*, 2011, **151**, 19–36.

92 X.-S. Wang, S. Ma, P. Forster, D. Yuan, J. Eckert, J. López, B. Murphy, J. Parise and H.-C. Zhou, *Angew. Chem., Int. Ed.*, 2008, **47**, 7263–7266.
93 J. F. Eubank, F. Nouar, R. Luebke, A. J. Cairns, L. Wojtas, M. Alkordi, T. Bousquet, M. R. Hight, J. Eckert, J. P. Embs, P. A. Georgiev and M. Eddaoudi, *Angew. Chem., Int. Ed.*, 2012, **51**, 10099–10103.
94 V. K. Peterson, Y. Liu, C. M. Brown and C. J. Kepert, *J. Am. Chem. Soc.*, 2006, **128**, 15578–15579.
95 V. K. Peterson, C. M. Brown, Y. Liu and C. J. Kepert, *J. Phys. Chem. C*, 2011, **115**, 8851–8857.